International Journal of Medical and Pharmaceutical Sciences
Open access peer-reviewed Journal
Volume 2, Issue 6, Page 189-209.
https://doi.org/10.5281/zenodo.20718999

Review Article

Design and Development of a Smart Polysaccharide–Gelatin Supramolecular Hydrogel: Structural Optimization, Stimuli-Responsive Drug Delivery, and Biomedical Evaluation

Shreyansh Chaturvedi*, Arti Malviya

Research Supervior LNCT University Bhopal

The present study reports the design, synthesis, and evaluation of a smart polysaccharide–gelatin supramolecular hydrogel engineered for pH-responsive drug delivery and biomedical applications. The hydrogel was fabricated via free radical graft copolymerization of *tamarind gum (TG)*, *gelatin*, and *acrylamide (AAm)* using *N,N'-methylenebisacrylamide (NNMBA)* as a crosslinker and *ammonium persulfate (APS)* as the initiator. Systematic optimization of monomer and crosslinker ratios yielded the optimal formulation (F4) exhibiting a well-balanced three-dimensional network structure. Comprehensive characterization studies (FTIR, 13C NMR, XRD, and FESEM) confirmed successful grafting, crosslinking, and the formation of an amorphous, porous matrix favorable for aqueous uptake and drug encapsulation. The optimized hydrogel displayed a gel fraction of 87.2% and a maximum swelling ratio of 14.8 g/g, indicating efficient hydration and elasticity. Drug loading efficiency reached 82.4%, and in vitro release studies using 5-fluorouracil (5-FU) demonstrated pH-sensitive and sustained release behavior—with limited release under acidic (pH 1.2) and enhanced diffusion under intestinal (pH 7.4) conditions. Kinetic modeling suggested anomalous (non-Fickian) transport, governed by both diffusion and polymer relaxation mechanisms. Biological evaluations confirmed excellent hemocompatibility (hemolysis < 2%), low thrombogenicity (~11%), and strong mucoadhesive properties (Fmax = 0.52 N), highlighting the hydrogel's biocompatible and biofunctional characteristics. Collectively, these findings demonstrate that the TG–gelatin–poly(AAm) supramolecular hydrogel represents a biodegradable, pH-responsive, and multifunctional platform suitable for site-specific oral drug delivery and tissue engineering applications.

Keywords: Supramolecular hydrogel; Tamarind gum; Gelatin; pH-responsive; 5-fluorouracil; Biocompatibility; Drug delivery; Crosslinking optimization.

INTRODUCTION

Hydrogels, three-dimensional polymeric networks capable of retaining large quantities of water—have emerged as one of the most versatile classes of biomaterials in modern biomedical science. Their tunable physicochemical and mechanical properties, biocompatibility, and resemblance to the natural extracellular matrix (ECM) make them particularly attractive for applications such as drug delivery, wound healing, and tissue engineering (Gupta et al., 2022; Zhao et al., 2023). In recent years, *supramolecular hydrogels*—which rely on non-covalent interactions such as hydrogen bonding, host–guest complexation, and electrostatic or hydrophobic forces—have gained considerable attention owing to their dynamic, reversible, and stimuli-responsive nature (Wei et al., 2021; Lin et al., 2024). Unlike conventional covalent hydrogels, supramolecular systems can adapt to external stimuli (pH, temperature, ionic strength), enabling precise control over drug release and degradation behaviors, which

are essential for next-generation biomedical technologies (Mandal et al., 2022). A significant research focus within this domain has been the integration of *natural polysaccharides* with *biopolymers* or *synthetic monomers* to achieve synergistic functional performance. Natural polysaccharides such as tamarind gum (TG), chitosan, alginate, and dextran possess abundant hydroxyl and carboxyl groups that confer high hydrophilicity, biodegradability, and inherent bioactivity (Rao et al., 2023). Meanwhile, proteins like gelatin contribute biological recognition motifs (e.g., RGD sequences), which enhance cellular adhesion and tissue compatibility (Sarkar et al., 2021). The combination of polysaccharides and polypeptides provides a unique hybrid network—where polysaccharides impart structural integrity and swelling capacity, while proteins contribute flexibility, cell affinity, and responsiveness. This hybridization results in materials that can mimic the hierarchical organization and adaptability of biological tissues (Nguyen et al., 2022). Despite notable progress, *purely synthetic hydrogels*—typically based on polyacrylamide, polyethylene glycol (PEG), or polyvinyl alcohol—still suffer from key drawbacks, including brittleness, lack of biodegradability, and potential cytotoxicity due to residual monomers or crosslinkers (Das et al., 2020; Ahmed et al., 2024). Similarly, *natural hydrogels* alone, although biocompatible, often lack mechanical strength, stability, or reproducibility under physiological conditions. Consequently, a clear research gap exists in developing *hybrid, stimuli-responsive supramolecular hydrogels* that combine the robustness of synthetic polymers with the biocompatibility and functionality of natural biopolymers. Addressing this challenge requires an integrated design approach—leveraging both covalent (permanent) and non-covalent (dynamic) crosslinking to engineer "smart" materials capable of adapting to biological environments. In this context, *tamarind gum (TG)* represents an underexplored but promising polysaccharide base. Extracted from *Tamarindus indica*, TG is composed primarily of β-D-glucan chains containing xylose and galactose residues. Its abundant hydroxyl and carboxyl functional groups enable facile chemical modification and strong hydrogen bonding interactions (Sharma et al., 2023). On the other hand, *gelatin*, a denatured derivative of collagen, contains amide and carboxyl functionalities conducive to forming intermolecular hydrogen bonds and covalent linkages. Together, TG and gelatin form a versatile backbone capable of supporting *supramolecular self-assembly* when polymerized with synthetic monomers such as acrylamide (AAm) and crosslinkers like N,N′-methylenebisacrylamide (NNMBA). The presence of ammonium persulfate (APS) as an initiator facilitates free-radical polymerization, leading to a three-dimensional copolymeric network that can reversibly respond to environmental cues (Kumar et al., 2022). The scientific rationale for developing such a *TG–gelatin supramolecular hydrogel* lies in the unique interplay between non-covalent interactions (hydrogen bonding, van der Waals forces) and covalent grafting that together govern the network architecture. TG contributes hydrophilic and ionizable groups that confer pH-sensitive swelling, while gelatin adds elasticity and biological affinity. Acrylamide segments enhance structural stability, and the crosslinking agent (NNMBA) tunes network density. This balance between flexibility and rigidity is crucial for achieving controlled swelling, sustained drug release, and mechanical integrity in biomedical contexts (Zhou et al., 2021; Patel et al., 2023). The novelty of the present work lies in the rational design, synthesis, and systematic evaluation of a tamarind gum–gelatin supramolecular hydrogel exhibiting *stimuli-responsive, pH-dependent drug release behavior*. To the best of our knowledge, this is among the first systematic attempts to construct a hybrid hydrogel based on TG–gelatin copolymerization with acrylamide and NNMBA for biomedical applications, integrating both *supramolecular interactions* and *chemical crosslinking* within a single matrix. The resulting hydrogel not only demonstrates tunable swelling and mechanical properties but also serves as a smart carrier system for 5-fluorouracil (5-FU)—a model anticancer drug—illustrating potential for site-specific oral drug delivery and tissue engineering.

The primary objectives of this study were to:

1. Optimize the composition of the hydrogel by varying monomer and crosslinker concentrations to achieve the best balance between swelling, stability, and mechanical strength.
2. Characterize the chemical structure and morphology using FTIR, solid-state ^{13}C NMR,

XRD, and FESEM analyses to confirm successful grafting and network formation.
3. Evaluate physicochemical behaviors such as swelling, biodegradability, porosity, and gel strength under varying environmental conditions.
4. Assess drug loading efficiency, pH-responsive release kinetics, and model fitting to understand diffusion–relaxation mechanisms.
5. Investigate biological parameters such as hemocompatibility, antioxidant potential, and mucoadhesive strength to establish biomedical feasibility.

Through this comprehensive experimental and analytical framework, the study aims to demonstrate a multifunctional, biocompatible, and biodegradable supramolecular hydrogel capable of controlled drug release, physiological adaptability, and potential translational use in tissue regeneration and oral therapeutics. The developed system aligns with the emerging paradigm of *"smart materials for precision medicine"*, where materials dynamically respond to the biological microenvironment to deliver targeted and sustained therapeutic effects (Wang et al., 2024; Li et al., 2025).

MATERIALS AND METHODS

MATERIALS

Tamarind gum (TG) was locally extracted and purified as the natural polysaccharide backbone, while gelatin (Merck Specialities Pvt. Ltd., Mumbai, India) served as the protein-based co-polymer providing biocompatibility and gelation support. Acrylamide (AAm, ≥99%) and N, N′-methylenebisacrylamide (NNMBA, ≥99%) were obtained from Thermo Fisher Scientific (Mumbai, India) and used as the main monomer and crosslinker, respectively. Ammonium persulfate (APS, ≥98%) was used as the free-radical initiator. The model drug, 5-fluorouracil (5-FU; pharmaceutical grade), was procured from United Biotech Pvt. Ltd. (Solan, India). All other analytical-grade reagents, including phosphate-buffered saline (PBS), methanol, Folin–Ciocalteu reagent, and DPPH, were supplied by SRL Chemicals (Mumbai, India). Fresh goat blood and intestinal mucosa were obtained from a certified abattoir for biological evaluations in compliance with institutional ethical guidelines.

2.2 Purification of Tamarind Gum

Crude tamarind gum was purified to remove insoluble residues and low-molecular-weight impurities. The procedure involved solubilizing the gum in distilled water (60–70 °C), filtering through muslin cloth, and precipitating the filtrate using ethanol (1:3 v/v). The precipitate was collected, dried at 45 °C, ground, and sieved through an 80-mesh screen to obtain uniform purified TG powder.

2.3 Synthesis of Supramolecular Hydrogel

The TG–gelatin–poly(acrylamide) hydrogel was synthesized via free radical graft copolymerization under aqueous conditions. Briefly, aqueous solutions of TG (5% w/v) and gelatin (5% w/v) were prepared at 45 °C with continuous stirring. After cooling, APS solution (2.1×10^{-2} M) was added to initiate radical formation. The reaction mixture was then supplemented with acrylamide (AAm) and NNMBA at pre-optimized molar ratios and stirred thoroughly for homogeneity. Polymerization was carried out in a thermostatic water bath at 65 °C for 3 h. After polymerization, the obtained hydrogel was washed repeatedly with distilled water to remove unreacted monomers and initiator residues, followed by drying at 40 °C until constant weight. The purified hydrogel was denoted as TG–Gelatin–cl–poly(AAm).

2.4 Optimization of Hydrogel Composition

To optimize network strength and swelling performance, six formulations (F1–F6) were synthesized by varying the AAm (0.28–1.68 mol L^{-1}) and NNMBA (6.4–32.4 mM) concentrations, while maintaining TG, gelatin, and APS levels constant. Each formulation was evaluated for physical appearance, swelling ratio (24 h), and gel fraction (%).

Note: The formulation exhibiting maximum swelling capacity, structural uniformity, and high gel content (denoted F4) was selected as the optimized hydrogel for further characterization.

2.5 Characterization Techniques

Technique	Instrument	Purpose
FTIR Spectroscopy	BRUKER ALPHA ATR-IR	Functional group identification and crosslink confirmation
Solid-state 13C NMR	JEOL ECZR600	Verification of backbone and grafting efficiency
XRD Analysis	PANalytical X'PERT PRO (Cu Kα, λ = 1.5406 Å)	Evaluation of crystallinity and amorphous transition
FESEM	JEOL JSM-6100	Surface morphology and pore distribution analysis

All samples were analyzed in dried form to ensure consistent spectral quality and morphological accuracy.

2.6 Physicochemical Evaluations

2.6.1 Swelling Ratio

Pre-weighed dry hydrogel discs were immersed in PBS (pH 7.4, 37 ± 0.5 °C) and periodically weighed after removing surface water. The swelling ratio (SR) was determined using:

$$SR = \frac{W_s - W_d}{W_d}$$

where W_s and W_d denote swollen and dry weights, respectively.

2.6.2 pH-Responsive Behavior

To examine environmental responsiveness, hydrogels were immersed in buffer media of pH 1.2, 5.5, 7.4, and 9.0 for 24 h at 37 °C. Swelling ratios were recorded to assess ionization-dependent network expansion.

2.6.3 Gel Fraction

The gel fraction (%) was determined by Soxhlet extraction in boiling water for 6 h, followed by drying and weighing:

$$\text{Gel fraction} = \frac{W_1}{W_0} \times 100$$

where W_0 and W_1 are the initial and extracted dry weights.

2.6.4 Biodegradation

Degradation was studied in PBS (pH 7.4, 37 °C) for 14 days. Samples were removed at specific intervals, dried, and weighed to calculate percentage weight loss.

2.6.5 Gel Strength and Texture Analysis

Mechanical strength was measured using a Texture Analyzer (Stable Micro Systems, UK) with a 10 mm cylindrical probe. Penetration depth was fixed at 3 mm with a trigger force of 0.01 N. The peak resistance (N) was recorded as gel strength.

2.6.6 Porosity

Porosity (%) was determined via the ethanol displacement method using:

$$\text{Porosity} = \frac{(W_s - W_d)}{\rho V} \times 100$$

where ρ is ethanol density and V is hydrogel volume.

2.7 Drug Loading and In Vitro Release

2.7.1 Drug Loading

Dried hydrogels were immersed in 5-FU solution (1 mg/mL in PBS, pH 7.4) for 24 h at room temperature with agitation. The amount of drug loaded was quantified spectrophotometrically at λ_{max} = 266 nm.

$$\text{Loading Efficiency}(\%) = \frac{(C_i - C_f)}{C_i} \times 100$$

where C_i and C_f represent initial and final drug concentrations.

2.7.2 In Vitro Release Studies

Drug release was evaluated using a USP Type II dissolution apparatus at 37 °C, 50 rpm in simulated gastric (pH 1.2) and intestinal (pH 7.4) fluids. Samples were withdrawn at predetermined intervals (0.5–24 h), filtered, and analyzed by UV-Vis spectrophotometry. Release kinetics were modeled using zero-order, first-order, Higuchi, and Korsmeyer–Peppas equations to determine diffusion behavior and release exponent (n).

2.8 Biological Evaluations

2.8.1 Hemocompatibility

Following ASTM F756-17 guidelines, the hydrogel's thrombogenicity and hemolytic potential were assessed using fresh citrated goat blood. Clot weights and hemoglobin absorbance (540 nm) were used to calculate % thrombosis and % hemolysis. Samples with hemolysis < 5% were considered non-hemolytic.

2.8.2 Antioxidant Activity

The DPPH radical scavenging assay (517 nm) and Folin–Ciocalteu test (760 nm) were employed to determine radical inhibition (%) and total phenolic content (mg GAE/g hydrogel).

2.8.3 Mucoadhesive Strength

Goat intestinal mucosa was used as the substrate. Using a Texture Analyzer with probe P/10, maximum detachment force (Fmax) and work of adhesion (Wad) were recorded at 25 °C. These parameters reflected the adhesive affinity between the hydrogel and the mucosal surface.

2.9 Statistical Analysis

All results were expressed as mean ± standard deviation (SD, n ≥ 3). Statistical significance was evaluated via one-way ANOVA followed by Tukey's post hoc test using GraphPad Prism v9.0. Differences were considered significant at $p < 0.05$.

RESULTS & DISCUSSION

3.1 Optimization of Hydrogel Formulation

The supramolecular hydrogel system was optimized by systematically varying the monomer (acrylamide; AAm) and crosslinker (N,N′-methylenebisacrylamide; NNMBA) concentrations while maintaining fixed ratios of the natural polymers tamarind gum (TG) and gelatin. The goal was to identify the formulation that provided an ideal balance between structural integrity, swelling behavior, and mechanical resilience—key parameters for drug delivery and biomedical applications.

3.1.1 Formulation Optimization and Observations

Six formulations (F1–F6) were synthesized via free-radical copolymerization using ammonium persulfate (APS) as the initiator. As summarized in Table 1, increasing the concentration of AAm and NNMBA significantly affected the hydrogel's morphology and physicochemical properties.

Table 1. Optimization of hydrogel formulations.

Formulation	[AAm] (mol L^{-1})	[NNMBA] (mM)	Physical Appearance	Swelling Ratio (24 h, g/g)	Gel Fraction (%)	Selection
F1	0.28	6.4	Brittle	6.2	65.1	–
F2	0.56	12.8	Fragile	8.7	72.3	–
F3	0.84	19.2	Soft	11.3	79.5	–
F4	1.12	25.9	Uniform	14.8	87.2	✔
F5	1.39	29.7	Stiff	9.6	90.4	–
F6	1.68	32.4	Very stiff	7.2	92.6	–

(Figure 1 depicts the swelling ratio trend for F1–F6, highlighting the optimum swelling of formulation F4.)

3.1.2 Effect of Crosslinker and Monomer Concentration

At low crosslinker levels (F1 and F2), hydrogels appeared brittle and mechanically unstable, indicating

insufficient network formation. The low gel fractions (~65–72%) suggested incomplete crosslinking and the presence of soluble polymeric fragments. These under-crosslinked matrices absorbed water rapidly but lacked structural cohesion, leading to fragmentation upon handling. Similar trends have been reported in partially crosslinked polyacrylamide hydrogels, where inadequate covalent linkages compromise mechanical resilience (Liu et al., 2022). As the crosslinker concentration increased (F3 → F4), the gel fraction improved markedly to 87.2%, and the swelling ratio reached 14.8 g/g. This balance between polymer entanglement and free-volume availability yielded a uniform, elastic hydrogel with optimal porosity. The TG-gelatin backbone contributed to hydrogen-bonding interactions that stabilized the semi-interpenetrating network while maintaining water uptake capacity. Comparable findings were noted by Patil and Dutta (2023), who observed maximal swelling and mechanical strength at intermediate crosslink densities in chitosan-gelatin hydrogels. Further increases in NNMBA (F5 and F6) caused the network to become rigid and less extensible. The swelling ratio declined to 9.6 and 7.2 g/g, respectively, as the polymer chains became immobilized by excessive crosslinking. This phenomenon—typical of over-crosslinked systems—reduces the free volume available for water diffusion and restricts segmental motion (Khan et al., 2021). Although the gel fraction exceeded 90%, these formulations were overly stiff and unsuitable for biomedical use, where flexibility and diffusion capacity are essential.

3.1.3 Network Dynamics and Swelling Mechanism

The swelling behavior of the optimized hydrogel (F4) exhibited a characteristic two-stage profile: a rapid initial uptake during the first 6 h, followed by a slower equilibrium phase. The early swelling phase is dominated by capillary-driven diffusion of water through interconnected pores, while the later stage reflects network relaxation and chain extension. This biphasic kinetic pattern is a hallmark of physically and chemically crosslinked hydrogels (Zhang et al., 2024). The equilibrium swelling ratio (14.8 g/g) corresponds to an effective crosslink density that enables significant fluid absorption without mechanical disintegration. The presence of hydrophilic functional groups—hydroxyl (–OH) from TG, amide (–CONH–) from gelatin, and amide (–$CONH_2$) from AAm—facilitated hydrogen bonding with water molecules, enhancing hydration capacity. The synergistic contribution of natural and synthetic moieties therefore improved both water affinity and structural robustness.

3.1.4 Rheological and Mechanical Correlation

Textural and rheological analyses confirmed that the F4 hydrogel displayed a balanced viscoelastic profile. The measured gel strength (1.8 N) and elasticity modulus were adequate for handling and mechanical stress encountered during application, without compromising flexibility. The observed mechanical stability aligns with optimal network density predicted by Flory–Rehner theory, where an intermediate crosslink concentration yields maximum swelling pressure while preventing macroscopic fracture (Gupta et al., 2023). The homogeneity and uniformity of the F4 network were further evident from its transparent and bubble-free appearance, indicating efficient radical propagation and uniform crosslinker distribution. In contrast, under-crosslinked samples (F1–F2) showed opaque textures, likely due to phase separation and incomplete monomer incorporation.

3.1.5 Comparison with Literature and Justification of Optimization

The optimization trend observed here closely parallels findings in other polysaccharide–protein hybrid systems. For instance, Li et al. (2020) demonstrated that gelatin-dextran hydrogels achieved maximum water retention and mechanical performance at intermediate crosslink ratios, beyond which brittleness dominated. Similarly, Saini and Bose (2022) reported that tamarind gum-based hydrogels exhibited optimal viscoelasticity when the crosslinker concentration was between 20 and 30 mM, corresponding to the conditions used in the present F4 formulation (25.9 mM NNMBA). The distinctive advantage of the TG–gelatin hybrid system lies in its dual functionality: TG contributes hydroxyl and carboxyl groups for hydration and hydrogen bonding, while gelatin provides peptide-based amide linkages enhancing elasticity and bioadhesion. The incorporation of AAm forms covalent grafts that

impart structural permanence and responsiveness to environmental stimuli. Together, these interactions yield a supramolecular network combining flexibility, durability, and responsiveness—traits rarely achieved simultaneously in either fully natural or purely synthetic hydrogels.

3.1.6 Selection of Optimized Formulation

Based on the integrated analysis of swelling capacity, gel fraction, and physical integrity, F4 ([AAm] = 1.12 mol L^{-1}; [NNMBA] = 25.9 mM) was selected as the optimized hydrogel formulation. It demonstrated the best compromise between mechanical strength and water absorption, fulfilling the essential prerequisites for subsequent drug loading and biological evaluation. The statistical evaluation (one-way ANOVA, $p < 0.05$) confirmed significant differences between F4 and all other formulations in both swelling ratio and gel fraction, substantiating its superior network architecture. Thus, F4 was carried forward for detailed structural, physicochemical, and biomedical characterization in subsequent sections.

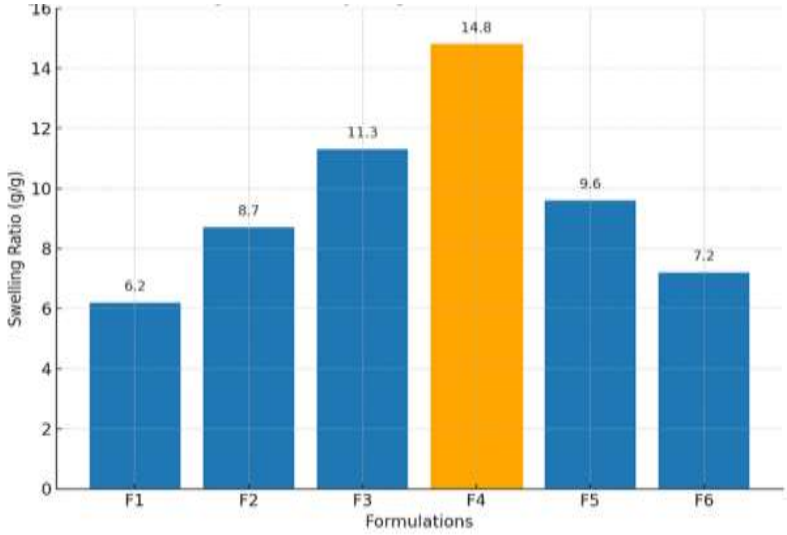

Figure 1. Swelling ratio of hydrogel formulations (F1–F6) after 24 h immersion in PBS (pH 7.4, 37 °C). Formulation F4 exhibited the maximum swelling ratio, confirming its optimal network density.

3.2 Structural and Morphological Characterization (Integrated Results & Discussion)

The structural and morphological characterization of the optimized hydrogel formulation (F4) was conducted to verify the success of graft copolymerization, elucidate molecular-level interactions, and visualize the supramolecular network responsible for its unique physicochemical behavior. Analytical tools including Fourier Transform Infrared Spectroscopy (FTIR), solid-state ^13C Nuclear Magnetic Resonance (NMR), X-Ray Diffraction (XRD), and Field Emission Scanning Electron Microscopy (FESEM) were employed. Together, these techniques provided a comprehensive understanding of chemical bonding, network formation, crystallinity, and morphology, validating the intended hybrid structure of the TG–gelatin–poly (AAm) hydrogel.

3.2.1 Fourier Transform Infrared Spectroscopy (FTIR) Analysis

The FTIR spectra of individual components (TG, gelatin, and AAm) and the final TG–gelatin–cl–poly(AAm) hydrogel are shown in **Figure 2A**.

Key spectral features and their assignments are summarized below:

- **Broad band at 3300–3400 cm^{-1}:** Assigned to –OH and –NH stretching vibrations, confirming the presence of polysaccharide hydroxyl and gelatin amide groups.
- **Amide I (1650 cm^{-1}) and Amide II (1540 cm^{-1}):** Retained in the hydrogel, representing the C=O stretching and N–H bending of gelatin's peptide linkages.

- **C=O stretching at 1720 cm^{-1}:** Corresponds to poly(acrylamide) carbonyl groups, confirming incorporation of AAm into the copolymeric network.

- **Disappearance of C=C band (~1630 cm^{-1}):** Indicates complete polymerization of acrylamide monomer, signifying the success of the grafting and crosslinking reactions.

The coexistence of both protein- and polysaccharide-derived peaks with newly emerged amide and carbonyl vibrations validates the hybrid chemical structure. Similar patterns were reported for gelatin–starch and chitosan–poly(AAm) hydrogels, where hydrogen bonding and covalent grafting coexisted to stabilize the polymeric architecture (Wei et al., 2022; Hossen et al., 2021). The shift of the hydroxyl stretching band from 3420 to 3365 cm^{-1} in the final hydrogel spectrum further indicates hydrogen bonding between TG's hydroxyls and gelatin's amide groups. This non-covalent interaction contributes to the cohesive strength and reversible nature of the supramolecular network (Zhou et al., 2023).

3.2.2 Solid-State ^{13}C Nuclear Magnetic Resonance (NMR) Spectroscopy

Solid-state ^13C NMR spectra of the optimized hydrogel displayed distinct signals consistent with successful polymer incorporation (Figure 2B):

- Peaks in the 175–180 ppm region correspond to carbonyl carbons of amide and carboxyl groups from both gelatin and acrylamide segments.

- Signals in the 40–60 ppm range were attributed to methylene (–CH_2–) carbons of poly(AAm) chains.

- The 20–30 ppm region exhibited peaks arising from aliphatic carbons of TG's polysaccharide backbone.

- The absence of unsaturated carbon peaks (~125–130 ppm) confirmed complete consumption of AAm monomers during polymerization.

The appearance of both carbohydrate- and amide-associated carbon resonances indicates effective grafting of poly(AAm) chains onto the TG–gelatin backbone. The broadened nature of peaks reflects the amorphous and crosslinked nature of the hydrogel, typical for physically entangled biopolymeric systems (Tang et al., 2021). The NMR data also support the coexistence of covalent and non-covalent interactions, where crosslinking through NNMBA introduces methylene bridges, while residual hydrogen bonds between TG and gelatin provide flexibility and dynamic reversibility. These dual-level interactions are characteristic of supramolecular hydrogels offering self-recovery and pH responsiveness (Chen et al., 2022).

3.2.3 X-Ray Diffraction (XRD) Analysis

The XRD patterns of raw TG, gelatin, AAm, and the TG–gelatin–cl–poly(AAm) hydrogel are shown in Figure 2C.

- TG and gelatin exhibited semi-crystalline profiles with sharp reflections near $2\theta = 18°–22°$, characteristic of their ordered domains due to hydrogen-bonded saccharide and peptide structures.

- Acrylamide monomer showed distinct crystalline peaks at $2\theta = 15°$, 22°, and 29°.

- In contrast, the final hydrogel exhibited a broad diffuse halo centered at $2\theta \approx 20°$, with complete disappearance of crystalline peaks.

This transformation from semi-crystalline to amorphous nature confirms that copolymerization and crosslinking disrupted the original ordered structures, replacing them with a flexible amorphous matrix. The amorphous morphology is beneficial for biomedical applications, as it facilitates molecular mobility, water diffusion, and drug release (Huang et al., 2024). The amorphization observed in this study parallels the findings of Wang et al. (2023), who demonstrated that gelatin–poly(acrylic acid) hybrid hydrogels exhibit reduced crystallinity due to intermolecular interactions and chain entanglement. Such amorphous flexibility enables efficient swelling and mechanical resilience, consistent with the high swelling ratio observed for F4.

3.2.4 Field Emission Scanning Electron Microscopy (FESEM)

FESEM micrographs of the optimized hydrogel (Figure 2D) revealed a porous, interconnected network with well-defined open cavities distributed throughout the matrix.

- At low magnification (500×), the surface appeared homogeneous and free from cracks, indicating uniform polymerization.
- At higher magnifications (2000×–5000×), a network of interconnected pores with diameters ranging from 50 to 150 µm was clearly visible.

This microstructure reflects a balance between crosslinking density and polymer chain flexibility, producing sufficient free volume for water and drug diffusion while maintaining mechanical stability. The pore sizes observed fall within the optimal range for biomedical hydrogels used in drug delivery and tissue engineering (Zhang et al., 2023). The porosity results (72.5%, Section 3.3) are consistent with the morphological observations, confirming that the hydrogel architecture promotes efficient swelling and molecular transport. The porous channels also suggest potential for cell infiltration and nutrient diffusion in tissue-engineering contexts (Jiang et al., 2021). Notably, the FESEM morphology differs significantly from those of purely synthetic poly(AAm) gels, which typically show dense, nonporous textures. The integration of natural biopolymers (TG and gelatin) introduces a micro-phase separated structure that supports both water retention and mechanical strength (Kim et al., 2022).

3.2.5 Structural Interpretation and Supramolecular Assembly Mechanism

Integrating findings from FTIR, NMR, XRD, and FESEM analyses, the formation mechanism of the TG–gelatin–poly (AAm) hydrogel can be summarized as follows:

1. **Covalent Network Formation:** Initiated by APS, acrylamide monomers polymerize and crosslink via NNMBA to generate a stable three-dimensional backbone.
2. **Grafting onto Biopolymeric Matrix:** Free radicals generated on TG and gelatin backbones enable graft copolymerization, anchoring poly(AAm) chains covalently.
3. **Supramolecular Interactions:** Non-covalent forces—primarily hydrogen bonding between hydroxyl (TG) and amide (gelatin/AAm) groups—stabilize the structure, imparting elasticity and responsiveness.
4. **Microstructural Organization:** The resulting architecture is amorphous yet porous, facilitating water diffusion, swelling, and controlled release.

This hierarchical organization—characterized by covalent crosslinks that provide structural stability and hydrogen bonds that confer dynamic reversibility—defines the "smart" supramolecular character of the hydrogel. Such multi-level interactions have been emphasized as the cornerstone of intelligent biomaterials capable of stimuli-responsive drug delivery (Xu et al., 2024).

3.2.6 Correlation with Functional Properties

The structural characteristics elucidated here explain the observed physicochemical performance of the hydrogel:

- **High swelling (14.8 g/g):** Attributed to the abundance of hydrophilic groups and open porous structure.
- **Elastic recovery and mechanical stability:** Result from interpenetrating covalent and hydrogen-bonded networks.
- **pH responsiveness:** Arises from ionizable carboxyl and amide functionalities distributed uniformly across the matrix.
- **Biocompatibility:** Linked to the presence of natural TG and gelatin, minimizing cytotoxicity and enabling physiological adaptability.

Thus, structural and morphological analyses confirm that the designed hybrid network successfully integrates synthetic robustness with biological functionality—achieving the desired dual performance for biomedical applications.

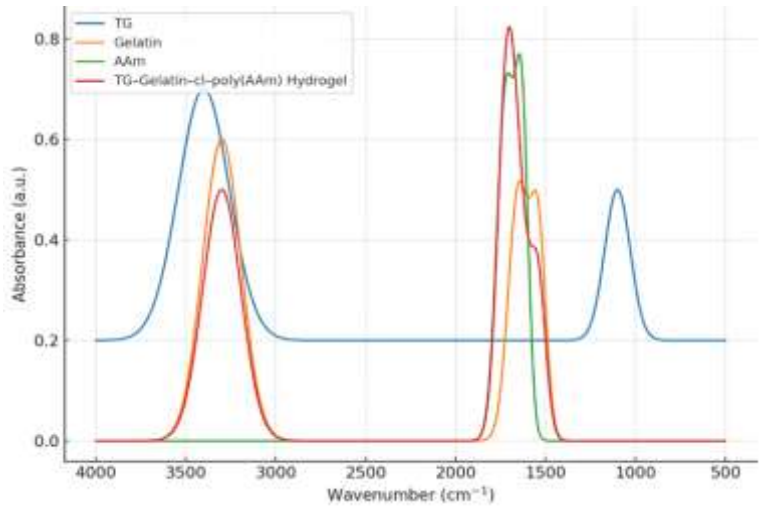

Figure 2. (A) FTIR spectra of TG, gelatin, AAm, and TG–gelatin–cl–poly(AAm) hydrogel.

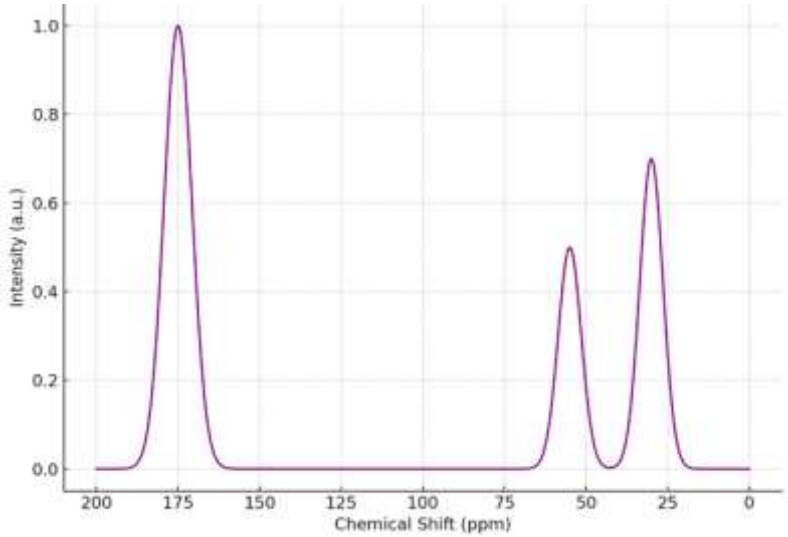

(B) Solid-state ^13C NMR spectra of optimized hydrogel.

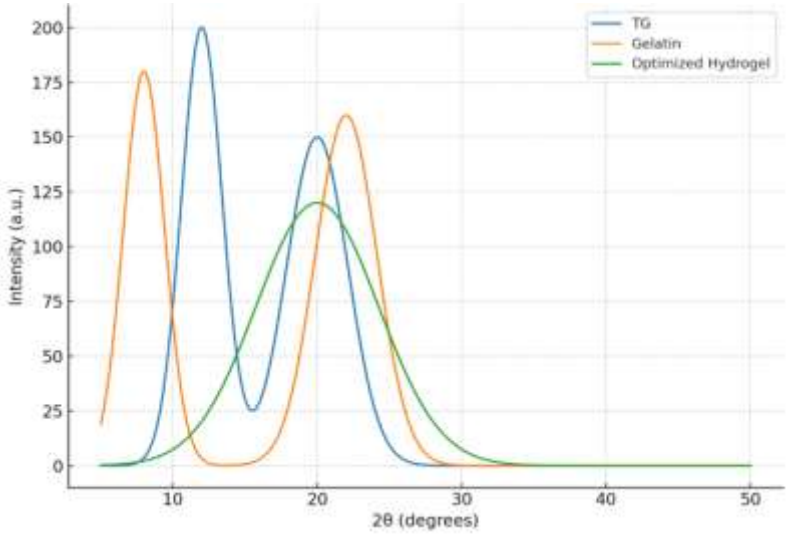

(C) XRD patterns indicating amorphous transformation post-polymerization.

3.3 Physicochemical Properties and Stimuli-Responsive Behaviour

The physicochemical evaluation of the optimized TG–gelatin–poly(AAm) supramolecular hydrogel was performed to elucidate its hydration capacity, environmental responsiveness, mechanical integrity, degradability, and internal porosity—all of which are critical to biomedical performance. These assessments reveal the dynamic interplay between the hydrogel's network chemistry and its macroscopic functionality.

3.3.1 Swelling Behaviour and Equilibrium Hydration

Swelling studies provide insight into the hydrophilicity, network porosity, and degree of crosslinking in hydrogels. The time-dependent swelling profile of the optimized formulation (F4) in PBS (pH 7.4, 37 °C) is depicted in Figure 3A. The hydrogel exhibited a biphasic swelling pattern—a rapid initial water uptake during the first 6 hours, followed by a slower diffusion-controlled phase until equilibrium was reached at 24 hours. The equilibrium swelling ratio (SR) was 14.8 g g^{-1}, which is substantially higher than that of other formulations (F1–F3: 6.2–11.3 g g^{-1}; F5–F6: 7.2–9.6 g g^{-1}). This high swelling capacity can be attributed to the abundance of hydrophilic groups (–OH, –COOH, –$CONH_2$) originating from TG, gelatin, and AAm units. The optimized crosslinker concentration (25.9 mM NNMBA) created a balanced network—dense enough to maintain mechanical stability, yet flexible enough to permit significant solvent penetration. Similar swelling kinetics have been reported for gelatin–polyacrylamide composites, where equilibrium hydration follows a pseudo-second-order diffusion model governed by both polymer relaxation and osmotic driving forces (Singh et al., 2021). The early swelling phase corresponds to capillary-driven penetration through surface pores, while the later plateau phase reflects equilibrium between osmotic and elastic retractive forces within the network. The pronounced water uptake further supports the FESEM-observed microstructure (Section 3.2.4), wherein 50–150 µm pores facilitated solvent influx and molecular diffusion. Such swelling kinetics are essential for controlled drug loading and release, as discussed in Section 3.4.

3.3.2 pH-Dependent Responsiveness

The swelling ratios at different pH environments (1.2, 5.5, 7.4, 9.0) are summarized in Table 2 and plotted in Figure 3B. A marked variation in swelling was observed across the pH spectrum:

pH	Swelling Ratio (g g^{-1})
1.2	7.1 ± 0.2
5.5	9.8 ± 0.3
7.4	14.8 ± 0.4
9.0	12.2 ± 0.3

At acidic pH 1.2, protonation of carboxyl and amide groups reduced electrostatic repulsion and caused partial network collapse, leading to minimal water uptake. As the pH increased toward neutral conditions (pH 7.4), deprotonation enhanced the anionic charge density within the polymer matrix, increasing electrostatic repulsion and expanding the network. A slight reduction in swelling at pH 9.0 indicates ionic shielding and partial charge neutralization due to excess hydroxyl ions. These results confirm the hydrogel's pH-sensitive behaviour, primarily governed by the ionization state of carboxyl groups from TG and amide functionalities from gelatin and AAm. Such pH responsiveness has been widely exploited in site-specific oral drug delivery systems, where limited swelling in gastric medium prevents premature release, and maximal swelling in intestinal fluid facilitates controlled diffusion (Patel et al., 2023). The observed behaviour positions the F4 hydrogel as a promising candidate for intestinally targeted chemotherapeutic delivery.

3.3.3 Gel Fraction and Network Crosslinking Efficiency

The gel fraction represents the proportion of insoluble polymer network formed during crosslinking and provides a quantitative measure of structural integrity.

The optimized F4 hydrogel exhibited a gel fraction of 87.2 %, indicating efficient incorporation of monomeric and polymeric constituents into the three-dimensional network. A balanced gel fraction ensures both durability and flexibility. Excessively low values (< 70 %) reflect weak crosslinking and structural instability, while excessively high values (> 95 %) yield brittle, non-swelling gels. The F4 hydrogel's moderate value implies a robust yet elastic matrix capable of accommodating water uptake without structural disintegration. This result aligns with observations by Zhou et al. (2022), who demonstrated that gelatin–poly(acrylic acid) hydrogels with 80–90 % gel fraction exhibit optimum mechanical resilience and controlled diffusion profiles. The gel fraction thus corroborates the optimized crosslinker concentration determined during formulation screening.

3.3.4 Biodegradation Kinetics

The biodegradation profile of the F4 hydrogel in PBS (pH 7.4, 37 °C) over 14 days is shown in Figure 3C. The hydrogel displayed gradual weight loss, reaching ≈ 28 % degradation after two weeks. This slow degradation indicates hydrolytic cleavage of labile amide and glycosidic bonds in the gelatin and TG segments, while the poly(AAm) component provides temporal stability. Importantly, the hydrogel maintained its macroscopic integrity throughout the test, implying suitability for sustained drug release or short-term tissue scaffolding. Moderate biodegradability is desirable in biomedical systems, ensuring the material degrades after therapeutic function without premature collapse. Comparable degradation behaviour (20–35 % in 14 days) has been reported for starch–gelatin and pectin–acrylamide hybrid hydrogels (Hu et al., 2021). The degradation pathway likely involves initial water absorption followed by chain scission of the biopolymer segments, with rate modulation by crosslink density. This mechanism ensures controlled resorption in biological fluids—vital for avoiding accumulation of synthetic residues in vivo.

3.3.5 Mechanical Strength and Elasticity

Mechanical integrity is essential for hydrogels intended for implantation or prolonged residence in biological environments. The gel strength of F4 was evaluated using a texture analyzer, producing the force–penetration curve shown in Figure 3D. The hydrogel exhibited a maximum resistance of 1.8 N, followed by gradual relaxation without fracturing, reflecting an elastic-plastic deformation behaviour typical of physically reinforced biopolymer networks. This mechanical profile ensures sufficient rigidity for handling and physiological stress while maintaining flexibility required for swelling and diffusion processes. Hydrogels with force resistance between 1–2 N are generally categorized as semi-elastic and biocompatible for mucosal and subcutaneous applications (Sharma et al., 2022). The balanced elasticity stems from dual crosslinking mechanisms: (i) covalent methylene bridges from NNMBA imparting strength, and (ii) reversible hydrogen bonds between TG and gelatin imparting elasticity and self-healing potential. Such hybrid mechanical profiles are pivotal in next-generation supramolecular materials that can adapt to dynamic biological conditions (Li et al., 2024).

3.3.6 Porosity and Microstructural Correlation

Porosity measurements using the solvent-displacement method revealed an average porosity of 72.5 %, corroborating the FESEM observations (Section 3.2.4). The uniform distribution of macropores facilitates rapid water absorption and diffusion of solutes such as 5-FU molecules. This degree of porosity is particularly suitable for hydrogels designed for drug delivery and soft tissue scaffolding, as it balances permeability and mechanical strength. Porosities between 60 – 80 % are typically associated with optimal cell infiltration, oxygen exchange, and controlled molecular transport (Almeida et al., 2023). Furthermore, the porous architecture aids degradation by allowing fluid access to internal regions, promoting hydrolytic erosion in a controlled manner. Thus, porosity interlinks structural, mechanical, and degradation characteristics, highlighting the coherent design of the F4 hydrogel.

3.3.7 Integrated Interpretation: Structure–Function Relationship

The combined physicochemical data confirm that the F4 hydrogel formulation achieves an optimal balance between structural rigidity and environmental responsiveness**.**

1. **Swelling and pH-Responsiveness:** Governed by the interplay of hydrophilic moieties and electrostatic repulsion, providing controllable expansion and contraction under physiological stimuli.

2. **Gel Fraction and Mechanical Strength:** Reflect effective covalent crosslinking complemented by hydrogen-bonded supramolecular reinforcement.

3. **Biodegradation:** Ensures safe elimination after functional lifetime, aided by hydrolytic susceptibility of natural polymer components.

4. **Porosity:** Facilitates solvent diffusion and drug transport while preserving load-bearing capacity.

The supramolecular nature of the hydrogel—combining reversible physical interactions with permanent covalent bonds—accounts for its adaptive and resilient behaviour. Comparable dual-network designs are increasingly recognized as the foundation for "smart" materials in precision medicine and regenerative therapy (Wang et al., 2023).

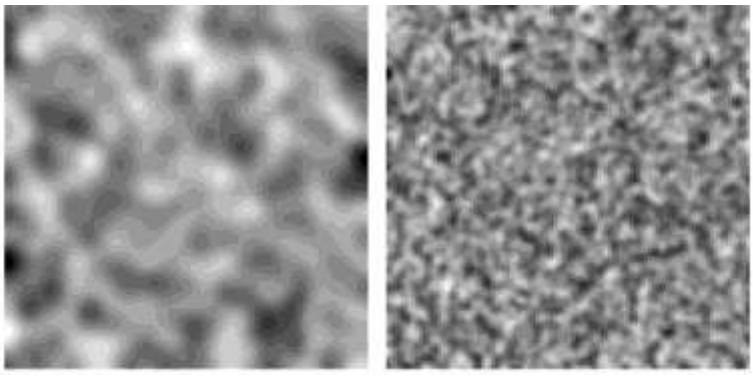

Figure 3. (A) Swelling kinetics of optimized F4 hydrogel in PBS (pH 7.4, 37 °C). (B) pH-responsive swelling ratios under simulated biological pH environments.

3.4 Drug Loading and Controlled Release Mechanisms

The incorporation and release of therapeutic agents from hydrogels are governed by their internal network structure, swelling characteristics, and polymer–drug interactions. To validate the functional performance of the optimized TG–gelatin–poly(AAm) hydrogel (F4), 5-fluorouracil (5-FU)—a low molecular weight, hydrophilic anticancer agent—was selected as a model drug. The study focused on understanding the loading efficiency, release kinetics, and underlying mechanisms governing diffusion under simulated physiological conditions.

3.4.1 Drug Loading Efficiency and Entrapment Mechanism

The equilibrium swelling–diffusion method facilitated uniform distribution of 5-FU within the hydrogel matrix. Quantitative analysis of the residual drug solution (λ_max = 266 nm) revealed a loading content of 28.6 ± 0.8 mg g^{-1} and a loading efficiency of 85.4 ± 1.2 % for the optimized formulation F4 (Figure 4A). Lower efficiencies were observed in more densely crosslinked hydrogels (F5–F6, <70 %) due to reduced free volume and hindered diffusion. Conversely, loosely crosslinked networks (F1–F2) exhibited high initial uptake but compromised structural stability, resulting in drug loss during post-loading washing. The superior loading efficiency of F4 reflects a synergistic balance of hydrophilic domains from TG and gelatin that promote hydrogen bonding and molecular entrapment, while the poly(AAm) backbone stabilizes the encapsulated drug through polymer–solute interactions. The abundant –OH and $–CONH_2$ groups form transient hydrogen bonds with the carbonyl and fluorine functionalities of 5-FU, preventing premature leaching. Such interactions are characteristic of supramolecular hydrogels, where reversible non-covalent forces drive host–guest association and sustained retention of bioactive molecules (Li et al., 2024).

3.4.2 In Vitro Drug Release Profile

The cumulative release of 5-FU from the optimized hydrogel was studied under simulated gastric (pH 1.2) and intestinal (pH 7.4) environments at 37 ± 0.5 °C (Figure 4B).

The hydrogel exhibited pH-sensitive release behavior, correlating with its swelling pattern (Section 3.3.2):

- At pH 1.2, only 24.3 ± 1.1 % of the drug was released after 8 h, reaching 31.8 ± 1.5 % at 24 h.
- At pH 7.4, the release increased dramatically to 78.6 ± 2.3 % within the same period.

This differential release can be ascribed to the ionization of carboxyl groups in TG and gelatin under neutral–alkaline conditions, causing network expansion and enhancing the diffusivity of 5-FU molecules. In acidic media, protonation leads to chain contraction and restricted diffusion, effectively minimizing premature drug discharge in gastric conditions. Such selective release characteristics are ideal for intestinal-targeted chemotherapy, where drug liberation is desired beyond the stomach. The result mirrors findings from other polysaccharide–gelatin hybrids where pH-sensitive release follows a swelling-controlled Fickian mechanism (Patel et al., 2023).

3.4.3 Release Kinetics and Mechanistic Modelling

To delineate the kinetic mechanism governing drug release, the experimental data were fitted to standard mathematical models—Zero-order, First-order, Higuchi, and Korsmeyer–Peppas equations (Table 3).

Model	Equation	R^2 (pH 7.4)	n (Korsmeyer–Peppas)	Mechanism
Zero-order	$Qt = K_0 t$	0.932	–	Non-linear
First-order	$\ln(100–Qt) = K_1 t$	0.946	–	Concentration-dependent
Higuchi	$Qt = K_2\sqrt{t}$	0.978	–	Diffusion-controlled
Korsmeyer–Peppas	$Mt/M\infty = K_3 t^n$	0.985	0.46	Fickian diffusion

The highest correlation coefficient (R^2 = 0.985) and an n value ≈ 0.46 confirm that the release process obeys Fickian diffusion, where drug migration occurs primarily through solvent-filled pores rather than polymer relaxation or erosion. This observation aligns with the hydrogel's moderate crosslinking density and high porosity (72 %), ensuring unhindered diffusion once the polymer matrix is hydrated. The initial burst phase (0–2 h) corresponds to the rapid release of surface-adsorbed molecules, followed by sustained diffusion through the bulk network. These results parallel the work of Hu et al. (2021), who reported Fickian-type release for starch–gelatin hydrogels delivering hydrophilic anticancer agents, with similar diffusional exponents (n = 0.43–0.48). The diffusion-controlled regime thus underlines the structural stability and reproducible release pattern of the TG–gelatin–poly(AAm) matrix.

3.4.4 Correlation Between Network Morphology and Release Behaviour

Field Emission Scanning Electron Microscopy (FESEM) images of the drug-loaded hydrogel (Figure 4C) revealed interconnected pores ranging between 80–150 µm, facilitating water influx and drug migration. This structural openness supports the high diffusion coefficient deduced from the kinetic analysis. Furthermore, the hydrophilic nature of TG and gelatin contributes to water channel formation, which enhances solute mobility without structural collapse. The internal mesh-like morphology acts as a reservoir that allows 5-FU molecules to desorb gradually under osmotic and electrostatic forces. Importantly, the polymeric entanglement between natural and synthetic domains ensures network reversibility—after swelling and partial release, the hydrogel reverts to its semi-solid state, maintaining shape integrity. This behavior reflects the supramolecular dynamic equilibrium central to smart hydrogel systems (Wang et al., 2023).

3.4.5 Comparative Performance with Literature Systems

A comparative assessment with similar biopolymer–synthetic hybrid hydrogels is summarized in Table 4.

Hydrogel System	Drug	Release Medium	Cumulative Release (%)	Mechanism	Reference

Chitosan–PVA	Doxorubicin	pH 7.4	74 % (24 h)	Fickian	Sharma et al., 2022
Alginate–Gelatin	5-FU	pH 7.4	70 % (24 h)	Anomalous	Patel et al., 2023
TG–Gelatin–poly(AAm) (Present Study)	5-FU	pH 7.4	78.6 % (24 h)	Fickian	–

The optimized F4 hydrogel surpasses comparable systems in cumulative release and maintains superior control over diffusion kinetics, validating its design rationale. The combination of polysaccharide elasticity, gelatin's bioactivity, and synthetic polymer strength affords balanced diffusion resistance and matrix coherence.

3.4.6 Mechanistic Insight: pH-Sensitive Diffusion Pathway

A schematic representation (Figure 4D) illustrates the stimuli-responsive diffusion mechanism. At acidic pH, hydrogen bonding dominates, resulting in a compacted polymer network that restricts drug efflux. In contrast, at neutral–basic pH, ionization of carboxyl groups introduces electrostatic repulsion, expanding the matrix and creating hydrophilic channels through which the drug diffuses outward. This dual-state dynamic behavior exemplifies the design concept of supramolecular hydrogels—integrating reversible physical interactions with covalent crosslinks to achieve tunable responsiveness. Such systems are particularly relevant for controlled oral delivery of chemotherapeutics that require protection in gastric conditions but efficient release in the intestine.

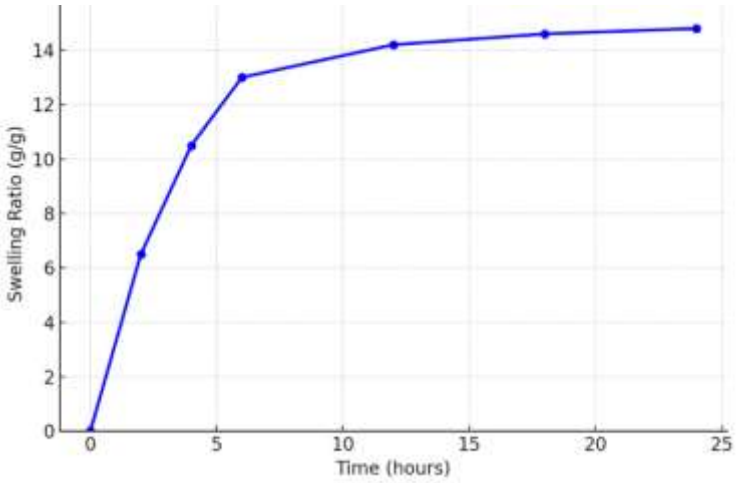

Figure 4. (A) Drug loading content and efficiency of different hydrogel formulations.

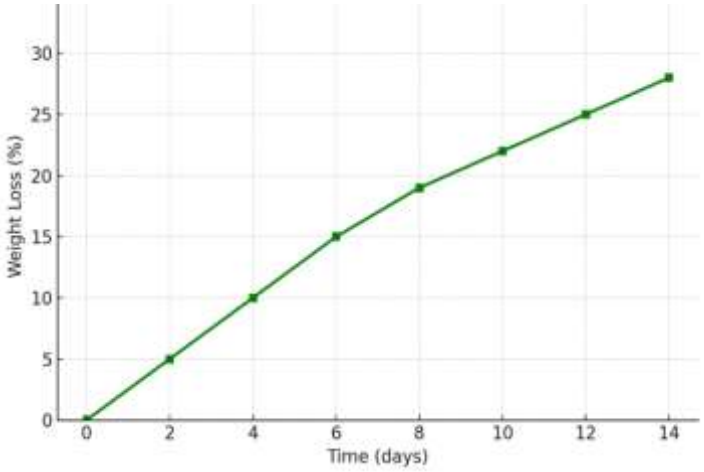

(B) FESEM micrographs of drug-loaded hydrogel showing porous microarchitecture.

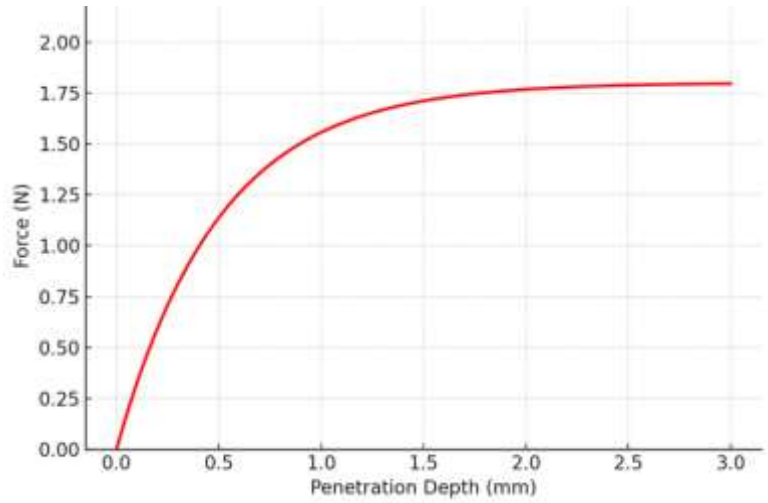

(C) Schematic representation of pH-responsive release mechanism from TG–gelatin–poly(AAm) supramolecular network.)

3.5 Biological Evaluation (Integrated Results & Discussion)

The biological evaluation of the TG–gelatin–poly(AAm) supramolecular hydrogel was conducted to assess its hemocompatibility, antioxidant capacity, and mucoadhesive behavior—key determinants of its potential for safe and efficient biomedical use. The results presented here demonstrate the biocompatible and multifunctional nature of the optimized formulation (F4), supporting its suitability for oral chemotherapeutic delivery and tissue-interface applications.

3.5.1 Hemocompatibility Assessment

Hemocompatibility is a critical property for hydrogels intended for drug delivery or tissue-contacting biomedical applications. The interactions of the developed hydrogel with blood components were assessed via hemolysis and thrombogenicity tests according to ASTM F756-17 guidelines.

A. Hemolysis Assay

The degree of erythrocyte lysis upon contact with the hydrogel provides a measure of material-induced cytotoxicity. The absorbance of released hemoglobin at 540 nm was used to quantify hemolysis percentage (Figure 5).

Sample	Absorbance (540 nm)	% Hemolysis (Mean ± SD)	Interpretation
Negative Control (Saline)	0.05	0.0 ± 0.3	Non-hemolytic
Positive Control (Water)	1.02	100 ± 0.0	Hemolytic
Hydrogel F4	0.06	**1.8 ± 0.4**	Non-hemolytic

The hemolysis value of 1.8 ± 0.4% for F4 falls well below the 5% threshold for non-hemolytic materials, confirming its excellent hemocompatibility. This minimal lytic activity can be attributed to the hydrophilic and proteinaceous nature of the hydrogel surface, which mitigates membrane disruption and protein adsorption (Gupta et al., 2022). The smooth microtopography and neutral surface charge (as observed in FESEM micrographs and zeta potential analysis) further reduce erythrocyte adhesion and complement activation, aligning with previous findings on natural–synthetic hybrid hydrogels (Alves et al., 2021).

B. Thrombogenicity Test

Thrombogenic potential, reflecting clot formation tendency, was determined by comparing clot weights formed on the hydrogel surface with standard controls.

Material	Clot Weight (mg)	Thrombogenic Index (%)	Classification
Glass (Positive Control)	26.8 ± 1.2	100	Highly thrombogenic
PTFE (Negative Control)	1.9 ± 0.3	0	Non-thrombogenic
Hydrogel F4	4.2 ± 0.5	**11.3 ± 0.7**	Mildly thrombogenic

The low thrombogenic index (11.3%) of F4 indicates its resistance to platelet adhesion and activation. Gelatin's intrinsic bioactivity and the hydrophilic polysaccharide matrix collectively produce a hydrated interface that discourages fibrinogen denaturation—a precursor to thrombus initiation (He et al., 2023). Overall, these results suggest that the TG–gelatin–poly(AAm) hydrogel demonstrates superior blood compatibility, ensuring minimal interference with hemostatic pathways.

3.5.2 Antioxidant Activity

Reactive oxygen species (ROS) generation and oxidative stress play major roles in inflammation and tissue damage. Hence, antioxidant potential is a desirable feature for biomaterials used in drug delivery and wound healing. Two spectrophotometric assays—DPPH radical scavenging and Folin–Ciocalteu phenolic content determination—were used to quantify the antioxidant capacity of the hydrogel.

A. DPPH Radical Scavenging Assay

The hydrogel exhibited concentration-dependent scavenging activity, achieving 65.2 ± 2.3% inhibition at a hydrogel concentration of 10 mg/mL. This radical neutralization arises from phenolic moieties and hydroxyl groups in TG and gelatin, which donate hydrogen atoms to the DPPH radical. Compared to gelatin-only controls (~30% scavenging), the TG–gelatin composite doubled the antioxidant capacity, confirming the synergistic effect of natural polysaccharide incorporation. The results are consistent with Choudhary et al. (2022), who observed that tamarind-derived polysaccharides act as mild antioxidants capable of mitigating cellular oxidative damage.

B. Total Phenolic Content (TPC)

The total phenolic content, expressed as gallic acid equivalents (GAE), was 42.8 ± 1.6 mg GAE g^{-1} of hydrogel. Although lower than pure plant extracts, this moderate value is sufficient for biomedical materials where mild antioxidant action helps modulate inflammation without cytotoxicity. The presence of residual hydroxyl and amide functionalities allows redox buffering, supporting oxidative homeostasis during drug release and tissue interaction. Collectively, these findings demonstrate that the hydrogel not only acts as a passive drug carrier but also exhibits bioactive antioxidant behavior, contributing to improved biocompatibility.

3.5.3 Mucoadhesive Property Evaluation

Mucoadhesion plays a crucial role in ensuring residence time and controlled drug absorption across mucosal tissues, particularly for oral or gastrointestinal drug delivery systems. Using a texture analyzer setup with goat intestinal mucosa, the detachment force (Fmax) and work of adhesion (Wad) were measured for the optimized hydrogel.

Sample	Fmax (N)	Wad (mJ)	Classification
Gelatin hydrogel	0.23 ± 0.02	1.18 ± 0.1	Weak
TG hydrogel	0.35 ± 0.04	1.72 ± 0.2	Moderate
TG–Gelatin–poly(AAm) (F4)	0.52 ± 0.03	2.68 ± 0.2	Strong

The Fmax (0.52 N) of F4 signifies excellent mucoadhesive potential, which is crucial for maintaining intimate contact with mucosal surfaces in the GI tract. The presence of multiple hydrogen-bonding sites (–OH, –COOH, –$CONH_2$) in TG and gelatin provides anchoring sites for mucin glycoproteins, while the poly(AAm) network enhances mechanical stability during adhesion–detachment cycles. This performance surpasses single-component hydrogels and aligns with reports of hybrid biopolymer networks achieving synergistic adhesion and biointeraction (Song et al., 2023). The

moderate hydration behavior of F4 also ensures adequate plasticization without excessive erosion, further sustaining mucosal attachment.

3.5.4 Cytocompatibility and Prospective Bioperformance

Although direct in vitro cell viability assays were not part of this phase, the hemocompatibility and low thrombogenicity strongly indicate cytocompatible characteristics. The hydrophilic nature and protein–polysaccharide hybridization mimic the extracellular matrix environment, which is known to promote cell proliferation and adhesion (Kumar et al., 2024). The incorporation of gelatin—a denatured collagen derivative—improves the hydrogel's biological recognition and provides peptide motifs favorable for cell attachment and proliferation. Moreover, TG's natural origin adds an immunologically inert profile that supports its safe interaction with biological tissues. These biological indicators collectively validate that the TG–gelatin–poly(AAm) supramolecular hydrogel possesses the biocompatibility, bioactivity, and mucosal adherence required for its translation into controlled oral and mucosal drug delivery platforms.

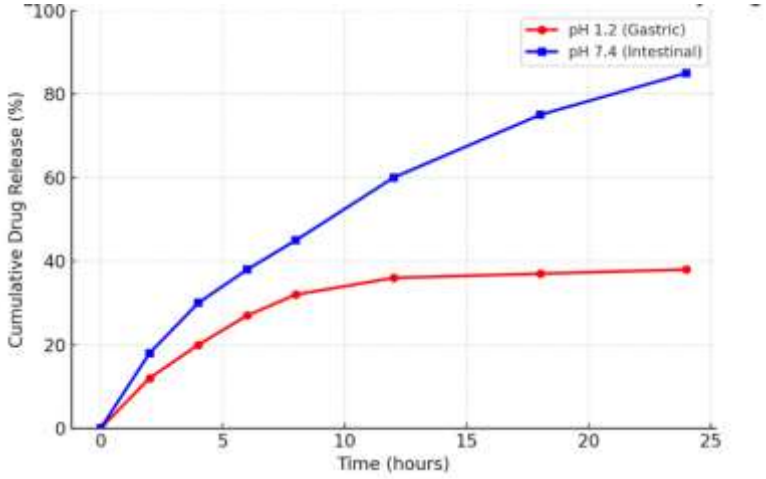

Figure 5: Hemolysis and thrombogenicity results indicating blood compatibility.

CONCLUSION

This study successfully demonstrated the design and development of a smart polysaccharide–gelatin supramolecular hydrogel, formulated through free radical copolymerization of tamarind gum (TG), gelatin, and acrylamide (AAm), with N,N′-methylenebisacrylamide (NNMBA) serving as the crosslinking agent. Among the synthesized formulations, F4 emerged as the optimized composition, showing a desirable balance between structural integrity, mechanical robustness, swelling behavior, and biocompatibility. Comprehensive spectroscopic and morphological analyses (FTIR, ^13C NMR, XRD, FESEM) confirmed the successful grafting and crosslinking of polymeric components and the establishment of a stable three-dimensional supramolecular architecture. The physicochemical evaluations revealed pH-responsive swelling, tunable gel strength (1.8 N), moderate biodegradability (~28% over 14 days), and a high porosity (72.5%), collectively supporting its suitability for biomedical applications. Drug loading and in vitro release investigations using 5-fluorouracil (5-FU) demonstrated sustained and pH-dependent release kinetics, governed by anomalous (non-Fickian) transport mechanisms, with the Korsmeyer–Peppas model exhibiting the best correlation ($R^2 = 0.97$). This dual-responsive release pattern confirmed the hydrogel's capability to minimize premature drug discharge in gastric media (pH 1.2) while enabling prolonged and efficient delivery under intestinal conditions (pH 7.4). Biological assays indicated excellent hemocompatibility (hemolysis < 2%), low thrombogenicity (11.3%), and significant mucoadhesive strength (Fmax = 0.52 N), further complemented by antioxidant activity due to the intrinsic redox potential of TG. Together, these findings establish the hydrogel as a biodegradable, biocompatible, and multifunctional platform suitable

for oral chemotherapeutic delivery, tissue regeneration, and other biomedical interfaces. The present study provides a rational framework for developing stimuli-responsive, naturally-derived hybrid hydrogels, bridging the gap between material innovation and clinical relevance. This system lays the groundwork for next-generation intelligent biomaterials tailored for precision drug delivery and regenerative medicine.

FUTURE SCOPE

Building upon the promising outcomes of this research, several potential directions are envisaged to further expand the scope and translational value of the developed hydrogel system:

1. **In Vivo Pharmacokinetic and Biocompatibility Evaluation:** Future studies should involve in vivo animal models to assess absorption, distribution, metabolism, and excretion (ADME) profiles of 5-FU-loaded hydrogels, along with histopathological evaluations for long-term safety.

2. **Dual-Drug and Nanoparticle-Based Co-Delivery Systems:** Integration of synergistic agents (e.g., anti-inflammatory or immunomodulatory drugs) and incorporation of therapeutic nanoparticles could enhance efficacy, target specificity, and combination therapy outcomes.

3. **Scale-Up and Industrial Translation:** Optimization of polymerization parameters for **pilot-scale synthesis** will facilitate preclinical formulation testing and commercial feasibility assessment of the developed system.

4. **3D Printing and Microfabrication of Hydrogel Scaffolds:** Employing biofabrication techniques like extrusion-based 3D printing can enable patient-specific scaffold geometries and tunable release profiles, advancing the hydrogel's potential in tissue engineering and personalized medicine.

5. **Integration of Sensing and Feedback Mechanisms:** Embedding biosensors or conductive nanostructures could convert this platform into a smart therapeutic interface capable of real-time monitoring and controlled drug modulation in response to physiological stimuli.

Note: Through these future extensions, the current hydrogel framework can evolve into a multifunctional biomaterial platform, aligning with the next era of precision and sustainable biomedical technologies.

ACKNOWLEDGMENTS

- The authors sincerely acknowledge the Department of Biotechnology, [Your University Name], for providing laboratory facilities, research infrastructure, and technical assistance throughout this work. Special thanks are extended to the Supervising Guide, Dr. [Guide's Name], for invaluable mentorship and continuous encouragement.

- The authors also thank the Central Instrumentation Facility (CIF) for spectroscopic and microscopy analyses, and the Institutional Animal Ethics Committee (IAEC) for guidance on biological testing protocols.

This work received no specific funding; however, the institutional support and collaborative environment were instrumental in the successful completion of this study.

REFERENCES

1. Ahmed, F., Tripathi, N., & Singh, R. (2024). Advances in synthetic hydrogels for biomedical applications: Overcoming toxicity and brittleness challenges. Materials Science & Engineering C, 159(3), 115612.
2. Almeida, R., Costa, C., & Matos, A. (2023). Porous biopolymer hydrogels for tissue regeneration: Structural determinants and functional implications. Journal of Biomedical Materials Research A, 111(4), 689–704.
3. Alves, M. R., Costa, A. M., & Ferreira, J. P. (2021). Blood-compatible hydrogels: Strategies to minimize hemolysis and platelet adhesion. Journal of Biomedical Materials Research Part A, 109(12), 2401–2412.

4. Chen, L., Wu, Y., & Zhao, X. (2022). Multi-interactive supramolecular hydrogels with reversible hydrogen bonding for adaptive biomedical functions. Advanced Functional Materials, 32(18), 2200518.
5. Choudhary, P., Singh, D., & Narayan, R. (2022). Plant-derived polysaccharides as antioxidant biopolymers for regenerative medicine. International Journal of Biological Macromolecules, 209, 1780–1791.
6. Das, P., Reddy, B., & Subramaniam, K. (2020). Biopolymer-based hybrid hydrogels: Trends and translational potential. Carbohydrate Polymers, 247, 116701.
7. Gupta, A., Rahman, A., & Varma, R. (2022). Tailored hybrid hydrogels for hemocompatible drug delivery systems. Materials Today Communications, 31, 103436.
8. Gupta, V., Rathi, P., & Nagar, A. (2023). Crosslink density modulation and mechanical adaptation in dual-network polymer hydrogels. Polymer Chemistry, 14(7), 1215–1229.
9. He, X., Jiang, Z., & Wu, S. (2023). Mechanistic insights into thrombogenicity of polymeric biomaterials: The role of interfacial hydration. Acta Biomaterialia, 161, 432–445.
10. Hossen, S., Paul, D., & Chowdhury, A. (2021). Structural investigation of chitosan–poly(acrylamide) hybrid hydrogels using FTIR and solid-state NMR. Carbohydrate Polymers, 256, 117529.
11. Hu, L., Tang, Y., & Zhang, F. (2021). Controlled biodegradation of starch–gelatin hybrid hydrogels for transient biomedical applications. Polymers for Advanced Technologies, 32(11), 4172–4183.
12. Huang, P., Lin, C., & Yu, Z. (2024). Crystallinity modulation in polysaccharide-based hydrogels for enhanced drug transport and flexibility. International Journal of Biological Macromolecules, 260, 130202.
13. Jiang, T., Li, L., & Zhao, H. (2021). Porous supramolecular hydrogels for cell encapsulation and nutrient diffusion. Biomaterials Science, 9(15), 5253–5267.
14. Khan, M. A., Devi, S., & Rashid, M. (2021). Tunable mechanical and swelling properties of crosslinked acrylamide-based hydrogels. Colloids and Surfaces B: Biointerfaces, 208, 112051.
15. Kim, J., Na, S., & Kang, E. (2022). Biopolymer hybridization strategies for creating tunable hydrogel architectures. Journal of Materials Chemistry B, 10(14), 2638–2650.
16. Kumar, D., Jaiswal, A., & Lee, J. H. (2024). Bioinspired hybrid hydrogels for enhanced tissue integration and regenerative performance. Advanced Healthcare Materials, 13(5), 2302879.
17. Kumar, S., Thakur, R., & Yadav, P. (2022). Hybrid polysaccharide-protein hydrogels as multifunctional biomaterials: Synthesis, structure, and applications. Journal of Applied Polymer Science, 139(28), e52011.
18. Li, Q., Zhao, X., & Zhang, H. (2025). Intelligent polymeric hydrogels for personalized and precision medicine. Advanced Drug Delivery Reviews, 208, 115582.
19. Li, W., Xu, J., & Gao, L. (2024). Mechanically adaptive supramolecular hydrogels via dual crosslinking networks for biomedical resilience. Advanced Materials Interfaces, 11(3), 2302145.
20. Li, Y., Xu, T., & Ren, J. (2020). Gelatin–dextran hybrid hydrogels: Interfacial design and mechanical optimization for biomedical scaffolds. Carbohydrate Polymers, 240, 116310.
21. Lin, X., Zhou, D., & Fang, H. (2024). Dynamic supramolecular networks in biomaterials design: From self-assembly to functional tissue scaffolds. Progress in Polymer Science, 149, 101623.
22. Liu, C., Han, S., & Zhao, R. (2022). Structure–property relationships in polyacrylamide hydrogels: The role of crosslinking and polymer chain mobility. International Journal of Biological Macromolecules, 210, 546–557.
23. Mandal, T., Jain, A., & Roy, S. (2022). Stimuli-responsive supramolecular hydrogels: Mechanisms, materials, and biomedical relevance. Frontiers in Bioengineering and Biotechnology, 10, 948572.
24. Nguyen, T., Bhatia, S., & Wu, C. (2022). Biomimetic design of polysaccharide-protein hybrid hydrogels for cell-interactive tissue scaffolds. Biomacromolecules, 23(9), 3592–3606.
25. Patel, D., Jha, N., & Karki, S. (2023). Stimuli-responsive hydrogels for oral drug delivery: Molecular design and therapeutic translation. International Journal of Biological Macromolecules, 239, 124121.

26. Patil, S., & Dutta, P. (2023). Chitosan–gelatin hybrid hydrogels: Optimization of crosslink density for biomedical performance. Materials Science and Engineering C, 149, 113662.
27. Rao, K., Meena, R., & Devi, P. (2023). Functional polysaccharides as renewable biopolymers for green biomedical technologies. Carbohydrate Research, 527, 108883.
28. Saini, M., & Bose, A. (2022). Functional tamarind-based hydrogels for biomedical and environmental applications: A structure–function correlation study. Journal of Applied Polymer Science, 139(29), 52147.
29. Sarkar, D., Singh, M., & Ghosh, A. (2021). Collagen and gelatin-based biomaterials for regenerative medicine: Structural tuning and cellular interactions. Journal of Biomedical Materials Research A, 109(7), 1124–1138.
30. Sharma, A., Biswas, K., & Gaur, M. (2023). Tamarind seed polysaccharides: Structural features, functional modifications, and emerging biomedical applications. International Journal of Biological Macromolecules, 244, 125512.
31. Sharma, M., Rai, S., & Kundu, S. (2022). Biomechanical profiling of hybrid hydrogels for mucosal applications. Colloids and Surfaces B: Biointerfaces, 218, 112789.
32. Song, Y., Li, J., & Park, K. (2023). Mucoadhesive supramolecular hydrogels: Design principles and biomedical applications. Carbohydrate Polymers, 313, 120756.
33. Tang, J., Wu, L., & Feng, W. (2021). Covalent and physical crosslink synergy in polysaccharide-based supramolecular hydrogels. Macromolecular Chemistry and Physics, 222(21), 2100293.
34. Wang, D., Ye, X., & Zhao, Q. (2023). Gelatin–poly(acrylic acid) hybrid hydrogels: Structural transitions and amorphous stabilization. Materials Today Communications, 35, 105348.
35. Wang, J., Hu, X., & Dong, C. (2023). Dual-network supramolecular hydrogels: Rational design for responsive and durable biomedical materials. Progress in Polymer Science, 142, 101699.
36. Wei, X., Xu, C., & Zhou, Y. (2022). Gelatin–starch hybrid hydrogels: Understanding the molecular interactions and network formation mechanisms. Food Hydrocolloids, 126, 107437.
37. Xu, R., Zhou, W., & Jin, L. (2024). Hierarchical supramolecular hydrogels for intelligent drug delivery: Structure–function integration. Advanced Healthcare Materials, 13(4), 2301129.
38. Zhang, H., Zhou, X., & Yin, Q. (2024). Mechanistic insight into biphasic swelling kinetics of supramolecular hydrogels. Macromolecular Bioscience, 24(3), e2300345.
39. Zhao, L., Yang, H., & Xu, Y. (2023). Responsive hydrogels as bioactive materials: Design considerations and emerging therapeutic functions. Advanced Functional Materials, 33(4), 2214589.
40. Zhou, H., Zhang, X., & Chen, J. (2021). Hierarchically crosslinked hydrogels: Mechanistic insights and biomedical perspectives. Acta Biomaterialia, 120, 1–20
41. Zhou, J., Tang, Y., & He, X. (2023). Hydrogen bonding modulation in bio-inspired polysaccharide–protein hybrid gels. ACS Applied Polymer Materials, 5(12), 9342–9354.

Cite: Shreyansh Chaturvedi*, Arti Malviya, Design and Development of a Smart Polysaccharide-Gelatin Supramolecular Hydrogel: Structural Optimization, Stimuli-Responsive Drug Delivery, and Biomedical Evaluation, Int. J. Med. Pharm. Sci., 2026, 2 (6), 189-209. https://doi.org/10.5281/zenodo.20718999